Effect of initiation on detonation cells for a three step chain-branching scheme

Hua Qiu[a], Luc Bauwens[b], Cha Xiong[a]
[a]School of Power and Energy, Northwestern Polytechnical University, No127 West Youyi road, xi'an, Shaanxi,710072,China
[b] Department of Mechanical and Manufacturing Engineering, University of Calgary, 2500 University Drive NW, Calgary, Alberta,T2N 1N4, Canada

1 Introduction

Experimental observations have shown that most detonation waves are not planar, but exhibit a cellular structure that involves triple shock interactions [1], consistent with results from stability analysis [2,3]. Numerical simulation has provided the tool of choice in studying the cellular structure, mostly in two dimensions [4-7], but also in three dimensions [8], both for single step Arrhenius kinetics, and also for more complex models, e.g. [9,10]. While single step may not accurately describe real mixtures, difficulties remain using complex kinetics, possibly because available schemes may not accurately represent the conditions prevalent in detonation waves [11]. Cells obtained from simulations in relatively narrow channels typically adapt to the channel width even if weakly unstable, as shown in simulations in wide channels for single step kinetics [12-13]. The key feature of real kinetics that the single step model fails to represent even qualitatively is chain-branching. Furthermore, in many cases including hydrogen, the initiation mechanism is much slower than other steps. These aspects are at least qualitatively described in a model three step scheme originally proposed by Kapila [14] and used e. g. in [2, 3,15]. Here, results are presented from simulations in wide channels for the model three step scheme, with stiff and slow initiation, in which case it has been shown [15] that in the ZND wave, moving toward termination chain branching eventually no longer takes place, leading to a potentially significant concentration of reactants that only burn very slowly under the combined effect of initiation and termination, so that for a practical purpose the reaction effectively stops. Results below consider mainly increasing values of the initiation activation energy and an increasing initiation length, mainly for CJ waves. Size and pattern of detonation cell are shown as numerical smoke foils. Results typically show that stiffer initiation leads to more irregular cells.

2 Physical Model and Numerical Scheme

The flow is described by the two-dimensional inviscid, non-conducting reactive Euler equations, for an ideal gas with constant specific heats. The kinetic scheme is the classical three step chain-branching model originally proposed by Kapila [14], which has been used in numerous studies, such as [15]. Initiation and branching are described by an Arrhenius model, while termination is constant. Heat release (Q) is associated with termination only. The problem is made dimensionless with respect to the pre-shock

Correspondence to: qiuhua@nwpu.edu.cn

state 0. Thus ρ,p,T,u,e are scaled by by ρ_0,p_0,T_0,$(c_0/\sqrt{\gamma})$,c_0^2/γ. Time is scaled by tc such that the constant termination rate is unity. Length is scaled by $tc(c_0/\sqrt{\gamma})$. Thus, the dimensionless scheme scheme is

$$r_I = \lambda_1 \tilde{K}_I \exp(-E_I / T), \tilde{K}_I = K_I \cdot t_C,\ K_I = \exp(E_I / T_I) \tag{1}$$

$$r_B = (p/T)\lambda_1\lambda_2 \tilde{K}_B \exp(-E_B / T),\ \tilde{K}_B = K_B \cdot t_C \rho_0,\ K_B = \exp(E_B / T_B) \tag{2}$$

$$r_T = \lambda_2 \cdot t_C \tag{3}$$

$$q = (1-\lambda_1-\lambda_2)Q \tag{4}$$

And λ_1 is the reactant mass fraction, λ_2 is mass fraction of the chain carrier and $(1-\lambda_1-\lambda_2)$ is the product mass fraction.The initial boundary value problem consists of the conservation laws of the reactive Euler problem on a rectangular domain. Initial conditions consist of a perturbed ZND profile. Uniform supersonic inflow on the left is consistent with the ZND profile, outflow on the right is approximately non-reflective and imposes a specified overdrive to the ZND wave. Top and bottom are slip walls. The perturbation consists of a sinusoidal disturbance added in the transverse velocity, uy immediately behind the shock. The disturbance is the same as in reference [16]. The problem above is solved numerically using flux functions are constructed using a third-order weighted essentially non-oscillatory scheme. Time integration uses a third-order accurate Runge–Kutta technique. An MPI based parallel has been implemented. The code has been used in a number of studies [15-17] and it is well-validated.

A domain size of $50x50L_{1/2}$ was used, where $L_{1/2}$ is the length measured from leading shock until half of the total heat is released in the ZND profile. 64 or 80 grids points per $L_{1/2}$ are used as required by a resolution study. Fresh mixture enters the domain supersonically at x = 0 while burnt mixture exits the domain at $x=50L_{1/2}$. The flow field is initialized at t=0 with the ZND profile.

3 Results

The chain-initiation step depends upon two parameters, either E_I and T_I or E_I and K_I. Two first sets of results were obtained for the corresponding two series of cases, thus maintaining T_I=4.6 constant while respectively varying E_I or K_I . In all simulations, γ=1.2, E_B= 2.5 and T_B = 2. Then the influence of the overdrive and the heat release were examined.

3.1 Results varying E_I with constant T_I

Fig.1 shows the effect of E_I on the ZND wave, for an overdrive f=1 and heat release Q=4. In all cases the x axis in Fig.1 is scaled by $L_{1/2}$ (The cut at x=16 corresponds to a change in the x scale on the figure). The values of $L_{1/2}$ for different values of E_I are shown in Table 1, which shows $L_{1/2}$ increasing with E_I. The length of the heat release zone $L_{h,r}$ (projection distance on x axis of the maximum-slope tangent line to the λ_3 profile from λ=0 to λ=1) scaled by $L_{1/2}$ is also given in Table 1. Although $L_{h,r}/L_{1/2}$ decreases as $L_{1/2}$ increases, the unscaled value of $L_{h,r}$ for different E_I remains around 4. For the current chain-branching mechanism, $L_{h,r}$ is mainly controlled by the chain-branching step while $L_{h,r}$ also changes with E_I for single step models. The induction length L_{ind}, defined as the length up to the peak in λ_2, increases with increasing E_I just as with single step kinetics. For E_I=8, the peak in λ_2 is 0.2128, which is the highest of all cases, and it appears at $x=0.8L_{1/2}$. As E_I increases, the peak in λ_2 drops slowly and the respective position shifts to the right. For E_I=8, the gradient in λ_2 (=$|d\lambda_2/dx|$) is below 0.0001 for $x> 16.82L_{1/2}$ while λ_1=0.005 at $x=16.82L_{1/2}$ and for E_I=30, the gradient in λ_2 is below 0.0001 for x>2.73L1/2 and λ_1=0.169 for $x=2.73\ L_{1/2}$. There remains a significant mass fraction of unburnt reactant at $x=50L_{1/2}$ for E_I>8, as shown in Table 1, reaching 0.16 at E_I=30 as pointed out already in [12].

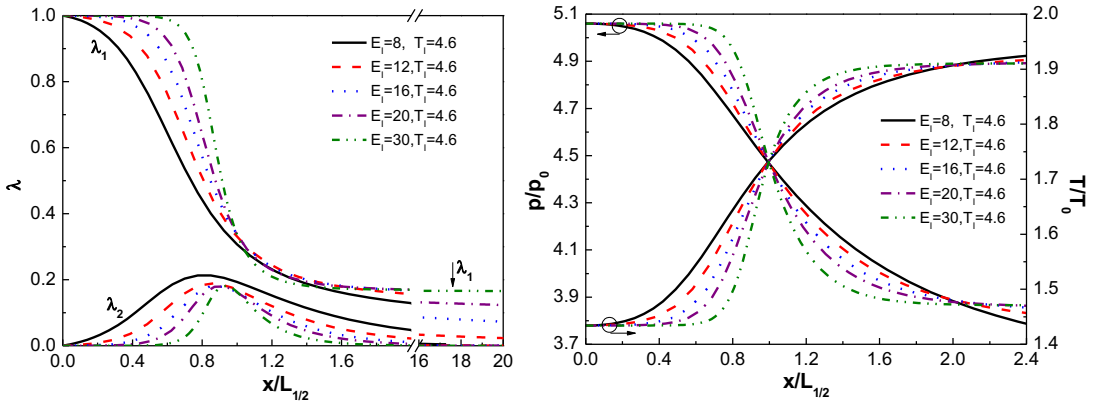

a) mass fractions in the ZND b) pressure and temperature in the ZND

Fig.1 ZND profile for T_I=4.6

Table.1 Half-reaction and heat-release zone length and cell size (T_I=4.6, f=1, Q=4)

	E_I=8 K_I=5.69	E_I=12 K_I=13.58	E_I=16 K_I=32.4	E_I=20 K_I=77.31	E_I=32 K_I=1050
$L_{1/2}$	2.891	4.124	5.299	6.422	9.304
$L_{h,r}/L_{1/2}$	1.17	0.96	0.79	0.65	0.45
$L_{ind}/L_{1/2}$	0.395	0.51	0.59	0.67	0.77
$L_{\lambda 2=peak}/L_{1/2}$	0.8	0.85	0.88	0.92	0.94
$\lambda_{1,x=50L1/2}$	0	0.0018	0.022	0.076	0.16

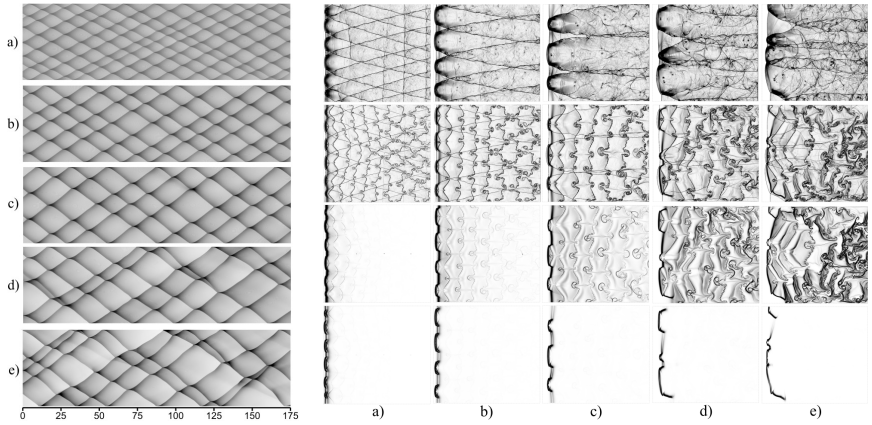

Fig.2 Numerical smoke foils(left) and Schlieren snapshots (right)with fixed T_I (domain 50×50$L_{1/2}$)
a) E_I=8; b) E_I=12; c) E_I=16; d) E_I=20; e) E_I=30.

Fig.2(left) shows the effect E_I on smoke foils for T_I=4.6, f=1, Q=4. Length is scaled by $L_{1/2}$. These are results from simulations carried out over a time long enough for the flow field to become approximately periodic. Resolution was 80 points per $L_{1/2}$ for E_I =30 and 64 points per $L_{1/2}$ for lower E_I, as determined by a convergence analysis. For E_I=8, 12 and 16 cells are fairly regular. There are 6 cells across the channel for E_I=8 hence a size of 8.3$L_{1/2}$. As E_I increases to 12, the size increases to 12.5$L_{1/2}$. And to 16.7 $L_{1/2}$ for E_I =16. For E_I =20 and 30 cells are less regular and the detonation is are more unstable. For E_I =20, cell numbers across oscillate between 2.5 and 3 cells, the largest size being 25$L_{1/2}$ and for E_I =30, between 3 and 3.5 cells across. The largest size then reaches 31$L_{1/2}$ while smaller cells appear between larger ones. Since $L_{1/2}$ increases with the E_I, the real size of the cells also increases.

Fig.2(right) shows typical numerical Schlieren snapshots at certain times with, from top to bottom, pressure, temperature, the mass fractions of reactants λ_1 and chain radicals λ2, for the same case of Fig.2(left). The entire computational domain is shown. Again, for E_I=8, 12, 16 the wave is more regular

than for E_I=20 and 30. The vortices seen in the temperature field become stronger as E_I increases. Unburnt fuel pockets appear for higher EI and chain-branching only occurs where the leading shock is strong.

The ZND profile is clearly very different from the real situation. For the λ_1 snapshots with E_I=30 in Fig.2, λ_1 is usually lower than 0.04 in the white regions behind the detonation front and importantly nearly completed reaction can also occur [15]. In the gray area, the reactant mass fraction reaches 0.46. Such a non-uniform energy release will make the detonation front more unstable and the flow field behind the front more complicated. Results for E_I=30 are very different from those of Bedard-Tremblay [15], who used similar chemical kinetics but in a narrow channel with $10L_{1/2}$ width and obtained regular cells structure and still large remaining unburnt reactants.

3.2 Results varying E_I with constant K_I

In this section, results for constant K_I=5.962 are shown that value is the same as in Table 1 for E_I=8 and T_I=4.6. When E_I increases, T_I now also increases, making K_I constant. The half-reaction and heat-release zone lengths are shown in Table 2. An increase in E_I, leads to $L_{1/2}$ also increasing and $L_{h,r}/L_{1/2}$ becomes shorter although $L_{h,r}$ remains around 4. Comparing the cases with the same E_I in Table 1 and Table 2, the reactions in Table 2 are more temperature-sensitive and exhibit longer reaction lengths. That reflects the influences of T_I or K_I on the reactions. The values of $L_{1/2}$ and $L_{h,r}$ at given E_I (eg. E_I=12) in Table 2 are between the values at the same E_I (eg. E_I=12) and the next larger E_I (eg. E_I=16) in Table 1. ZND profiles for the cases in Table 2 are similarly affected. More unburnt reactants remain at x=50$L_{1/2}$ for the same E_I. Compared with Table 1, $\lambda_{1,x=50L1/2}$ increases from 0.022 to 0.105 at E_I=16.

Table.2 Half-reaction and heat-release zone length and cell size (K_I=5.69, f=1, Q=4)

	E_I=8 T_I=4.6	E_I=12 T_I=6.9	E_I=16 T_I=9.2	E_I=20 T_I=11.5	E_I=30 T_I=17.25
$L_{1/2}$	2.891	4.6594	6.3201	7.9489	12.342
$L_{h,r}/L_{1/2}$	1.17	0.87	0.65	0. 52	0. 33
$L_{ind}/L_{1/2}$	0.395	0.55	0.66	0.73	0.83
$L_{\lambda 2=peak}/L_{1/2}$	0.8	0.86	0.89	0.92	0.96
$\lambda_{1,x=50L1/2}$	0	0.016	0.105	0.158	0.17

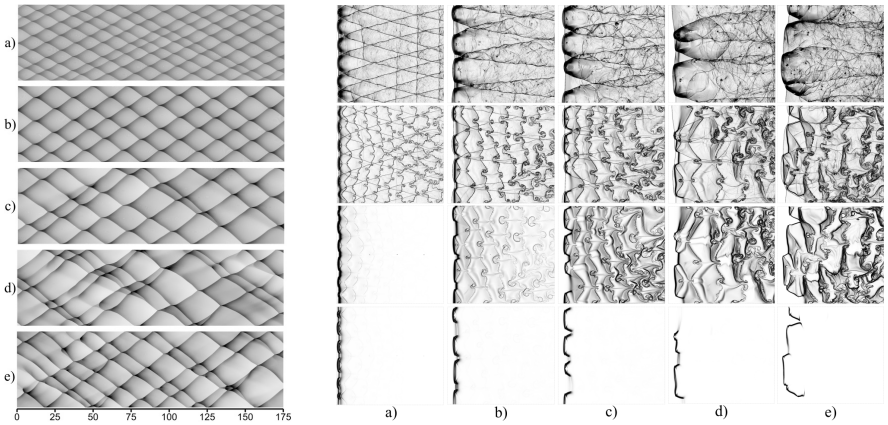

Fig.3 Numerical smoke foils(left) and Schlieren snapshots (right)with fixed K_I (domain 50×50$L_{1/2}$)
a) E_I=8; b) E_I=12; c) E_I=16; d) E_I=20; e) E_I=30.

Fig.3(left) shows the effect of E_I on smoke foils for K_I=5.692, f=1, Q=4. Again, simulations were carried out long enough results to become approximately periodic. Resolution was 80 points per $L_{1/2}$ for E_I =20, 30 and 64 points per $L_{1/2}$ for the other cases. Again, as E_I increases, the cells become larger and detonation becomes more unstable. Here, only for E_I=8 and 12 are the cells reasonably regular. There are 3.5 cells across for E_I=12 and the average cell size is 14.3$L_{1/2}$, which is larger than for the same E_I in Fig.2(left). As E_I increases to 16, the cells are larger and more unstable, oscillating between 2.5 cells and 3.5 cells across. Cells for E_I=20,30 are also less regular than in Fig.2. An increase of T_I or a decrease of K_I

results in larger and more unstable cells.Typical numerical Schlieren snapshot are also shown in Fig.3(right), with from top to bottom, pressure, temperature, λ_1 and λ_2. Only for E_I=8 and 12 is the wave reasonably regular. When E_I is greater than 12, vortices become stronger. Compared with Fig.3, more obvious unburnt fuel pockets appear at E_I=16. Non-uniform distribution of reactants λ_1 behind the front become more significantly with increasing E_I.

3.3 Influence of the overdrive and heat release

The cases above considered an overdrive f=1 and a heat release Q=4. They showed more unburnt reactants remaining for increasing E_I. To eliminate the influence of that issue on detonation stability, simulations for higher overdrive and higher heat release were carried out, still with T_I =4.6. The corresponding $L_{1/2}$ and λ_1 at x=50 $L_{1/2}$ of the ZND profile are shown in Table 3, showing that that $L_{1/2}$ and $\lambda_{1,x=50L1/2}$ decrease significantly.

Table.3 parameters of ZND and cell numbers along the width of domain (T_I=4.6)

	E_I=8	E_I=12	E_I=16	E_I=20	E_I=30	
$L_{1/2}$	1.6259	2.1025	2.5536	3.009	4.1175	f=1.4 Q=4
$\lambda_{1,x=50L1/2}$	0	0	0.002	0.01	0.036	
Cell numbers	5	5	5	4.5	4.5	
$L_{1/2}$	1.2604	1.5629	1.858	2.1503	2.891	f=1 Q=8.1548
$\lambda_{1,x=50L1/2}$	0	0	0	0.0003	0.0043	
Cell numbers	4.5	3.5	3	3	3	

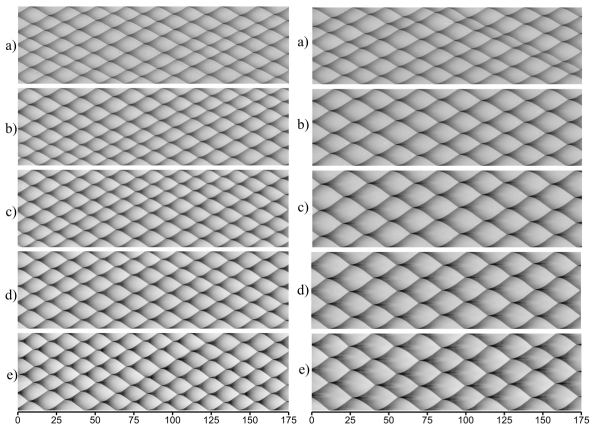

(I) f=1.4 and Q=4 (II) f=1 and Q=8.1548

Fig.4 Numerical smoke-foil records for fixed T_I=4.6
a) E_I=8; b) E_I=12; c) E_I=16; d) E_I=20; e) E_I=30.

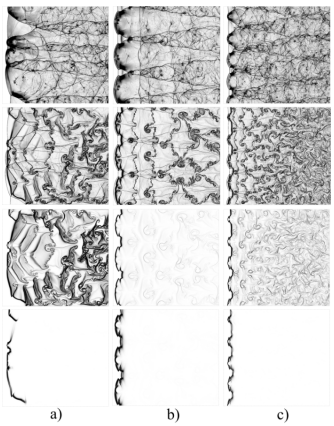

Fig.5 Numerical Schlieren snapshots with E_I=30 and T_I=4.6
a) f=1&Q=4; b) f=1&Q=8.1548; c) f=1.4&Q=4

Fig.4 shows the effect of E_I on smoke foils for the cases in Table 3. Length is scaled by $L_{1/2}$. Resolution was 80 points per $L_{1/2}$ for E_I =30 and 64 points per $L_{1/2}$ for lower E_I, as determined by a convergence analysis. In comparison with Fig. 2 and Fig. 3, the crucial difference is that detonations are only weakly unstable even for higher E_I. Although the increase of E_I still enlarges the cell size, the influence of E_I on the cell size scaled by $L_{1/2}$ is weaker. For example, cell sizes for E_I=16, 20 and 30 are all equal to 16.7 $L_{1/2}$ for f=1 and Q=8.1548.

Typical numerical Schlieren snapshots for cases E_I=30 and T_I=4.6 with different f and Q are shown in Fig. 5. The transverse wave structure for f =1.4 or Q=8.1548 can be categorized into double Mach configuration while that of f=1 and Q=4 are complex double Mach configuration. The strength of some parts of transverse wave is stronger than the Mach stem and the respective reaction induction length are different. For f=1 and Q=4, the strength of Mach stem is not enough to result in complete reaction, which only occurs far behind the Mach stem. This is clearly seen in the λ_1 plot, and may be associated with increased instability. For increasing overdrive f or heat release Q, the strength of Mach stem also increases which is enough to result in near-complete reaction close to the leading shock.

4 Conclusion

The detonation structure was examined for a model three-step chain-branching reaction including initiation, chain-branching and termination steps. To that effect numerical simulation were performed in a wide channel using a grid resolution fine enough that convergence was verified. The focus was on the effect of the chain-initiation step including its activation energy and rate multiplier. The length of the main heat release zone was found to be largely independent of initiation. However just as with single step Arrhenius models, an increased initiation length, either by increasing the initiation activation energy or by decreasing the rate multiplier results in a larger cell and a more unstable wave pattern on numerical smoke foils. Even if scaled by the half-reaction length, the cell size also increases. Results were similar whether increasing the activation energy and maintaining the rate multiplier K_I constant, or for constant T_I such that $K_I = \exp(E_I/T_I)$ although the latter results in a somewhat longer and more unstable wave, leaving a larger unburnt concentration behind.

Acknowledgement

This work was supported by National Natural Science Foundation of China under Grant number 51676164.

References

[1] W. Fickett and W. C. Davis, Detonation, University of California Press, Berkeley,1979.
[2] M. Short, J. W. Dold, Math. Comput. Modelling 24(8)(1996) 115-123.
[3] M. Short, J.J. Quirk, J. Fluid Mech. 339(1997) 89-119.
[4] E.S. Oran, J.P. Boris, T.R. Young, M. Flanigan, T. Burks, J.M. Picone,et al., Proc. Combust. Inst. 18 (1981) 1641-1649.
[5] K. Kailasanath, E.S. Oran, J.P. Boris, T.R. Young, Combust. Flame 61(3)(1985)199-209.
[6] A. Bourlioux, A.J. Majda, Combust. Flame 90(3-4) (1992) 211-229.
[7] V.N. Gamezo, D. Desbordes, Combust.Flame 116(1-2) (1999)154-165.
[8] D.N. Williams, L. Bauwens, Proc. Combust. Inst. 26(1996)2991-2998.
[9] J. Y. Choi, F. H. Ma, V. Yang, Combust. Explo. Shock. 44(5)(2008)560-578.
[10] E.S. Oran, J.W. Weber, E.I. Stefaniw, M.H. Lefebvre, J.D. Anderson, Combust. Flame 113(1–2) (1998)147–163.
[11] B.D. Taylor, D.A. Kessler, V.N. Gamezo, E.S. Oran, Proc. Combust. Inst., 34 (2) (2013) 2009-2016.
[12] M. Nikolic, D.N. Williams and L. Bauwens, in Gaseous and Heterogeneous Detonations, G. Roy, S. Frolov, K. Kailasanath and N. Smirnov, Editors, ENAS Publishers, Moscow, 1999, 153-161.
[13] G.J. Sharpe and J.J. Quirk, Combust. Theor. Mod., 12 (1) (2008) 1-21.
[14] A. K. Kapila, J. Eng. Math.12(3) (1978)221-235
[15] L. Bedard-Tremblay, J. Melguizo-Gavilanes, L. Bauwens, Proc. Combust. Inst. 32(2009)2339-2347.
[16] Z. Liang, L. Bauwens, Combust. Theor. Model. 9(1) (2005) 93-112.
[17] Z. Liang, L. Bauwens, Shock Waves, 15(3-4) (2006) 247-257.